Phonovoltaic. I. Harvesting hot optical phonons in a nanoscale p-n junction

Corey Melnick and Massoud Kaviany

Phonovoltaic: Part I – Harvesting hot optical phonons in nano-p-n junction

Corey Melnick and Massoud Kaviany*

University of Michigan

Department of Mechanical Engineering

Ann Arbor, MI 48105-2125

Abstract

The phonovoltaic (pV) cell is similar to the photovoltaic. It harvests nonequilibrium (hot) optical phonons ($E_{p,O}$) more energetic than the bandgap ($\Delta E_{e,g}$) to generate power in a p-n junction. We examine the theoretical electron-phonon and phonon-phonon scattering rates, the Boltzmann transport of electrons, and the diode equation and hydrodynamic simulations to describe the operation of a pV cell and develop an analytic model predicting its efficiency. Our findings indicate that a pV material with $E_{p,O} \simeq \Delta E_{e,g} \gg k_\mathrm{B}T$, where $k_\mathrm{B}T$ is the thermal energy, and a strong interband electron-phonon coupling surpasses the thermoelectric limit, provided the optical phonon population is excited in a nanoscale cell – enabling the ensuing local nonequilibrium. Finding and tuning a material with these properties is challenging. In Part II (this issue), we tune the bandgap of graphite within density functional theory through hydrogenation and the application of uniaxial strains. The bandgap is tuned to resonate with its energetic optical phonon modes and calculate the *ab initio* electron-phonon and phonon-phonon scattering rates. While hydrogenation degrades the strong electron-phonon coupling in graphene such that the figure of merit vanishes, we outline the methodology for a continued material search.

I. INTRODUCTION

Solid-state heat harvest, dominated by the thermoelectric (TE) generator[1], remains inefficient, and this limits its application to waste-heat recovery or hostile-environment power generation, where reliability supersedes efficiency. Moreover, TE effectiveness vanishes in nano and microscale devices, where the contact resistance dominates the thermoelectric effects[2-5]. These factors led to the development of the thermovoltaic (TV) cell by Span et. al.[6], wherein the hot-side p-metal-n junction in a TE is replaced by a p-n junction and electron generation events supply the TE current. They proposed that the TV can slightly exceed the limiting TE efficiency. However, subsequent investigation[7-10] indicated the TV cell achieves, at most, the TE efficiency.

Here, the phonovoltaic (pV) is proposed. While the pV and TV share a similar architecture, the pV utilizes a nonequilibrium optical phonon population to drive generation. Indeed, the pV shares more features with a photovoltaic (PV) cell than it does with a TE or TV cell. Where TE and TV harvest a flux of equilibrium energy carriers (heat), the PV and pV cells harvest nonequilibrium energy carriers (the photon and phonon, respectively) resonant with or more energetic than the bandgap, as shown in Fig. 1. Other nonequilibrium phonon harvesting schemes have received attention for their ability to surpass the TE limits in scale and efficiency. These include the laser cooling of ion-doped materials through anti-Stokes florescence[11,12], and the use of in-situ electron barriers to recycle phonons emitted during the Joule heating[13,14]. Conversely, the pV cell focuses on power generation.

In a pV cell, native, nonequilibrium (hot) phonons more energetic than the bandgap generate electron-hole pairs at rate $\dot{\gamma}_{e-p}$ (where $\dot{}$ is used to represent a rate), and a p-n junction separates them to produce power, as shown in Fig. 1. In comparison, a PV cell harvests imported, nonequilibrium photons more energetic than the bandgap to generate electrons. While excess photon energy is the primary source of entropy generation in a PV cell, both the excess phonon energy and the rate of optical phonon downconversion ($\dot{\gamma}_{p-p}$) into the acoustic phonon modes generate entropy in a pV cell.

Section V uses a band-to-band net generation model (A) in the diode equation to derive the current-voltage relationship (B) and the efficiency (C) in a pV cell. (D) The results of this derivation are summarized in Eq. (1), and illustrated in Fig. 5. To summarize, the extent of the local electron-phonon nonequilibrium (Carnot efficiency, η_C), the fraction of
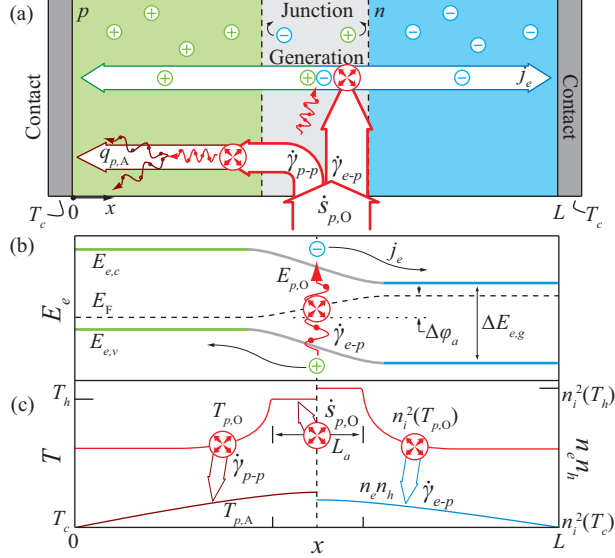
2

FIG. 1. (a) The phonovoltaic cell, (b) the energy diagram, and (c) nonequilibrium in terms of acoustic ($T_{p,A}$) and optical ($T_{p,O}$) phonon temperatures and the carrier concentrations (electron n_e, hole n_h, and intrinsic n_i). An external source excites the optical phonon population ($\dot{s}_{p,O}$) in the active region (L_a), and the resulting nonequilibrium drives generation ($\dot{\gamma}_{e-p}$) and downconversion into acoustic phonons ($\dot{\gamma}_{p-p}$). The junction separates generated electron-hole pairs to create a current (j_e) and potential ($\Delta\varphi_a$), i.e., power, while acoustic phonons conduct to the cold contacts (T_c).

the hot optical phonons which generate electrons ($\dot{\gamma}^*_{e-p}$) (Section III), and the fraction of phonon energy ($E_{p,O}$) preserved by the bandgap ($\Delta E_{e,g}$) determine the pV efficiency (η_{pV}) and its pV figure of merit (Z_{pV}), i.e.,

$$\dot{\gamma}^*_{e-p} = \frac{\dot{\gamma}_{e-p}}{\dot{\gamma}_{e-p} + \dot{\gamma}_{p-p}} \leq 1, \quad Z_{pV} = \dot{\gamma}^*_{e-p}\frac{\Delta E_{e,g}}{E_{p,O}} \leq 1 \quad , \quad \eta_{pV} \leq \eta_C Z_{pV}, \tag{1}$$

where the Carnot limit in a pV cell is determined by the difference in the hot optical phonon temperature, $T_{p,O}$, and the cold, contact temperature, T_c, i.e.,

$$\eta_C = \frac{T_{p,O} - T_c}{T_{p,O}}. \tag{2}$$

Few materials exist with an optical phonon mode more energetic than the bandgap[15], and even fewer exhibit an optical phonon significantly more energetic than $k_B T$ at room temperature, such that the p-n junction effectively separates generated carriers (where k_B is the Boltzmann constant). However, graphite (graphene), with a phonon cut-off energy of

3

198 meV[16,17], phonon linewidth dominated by the electron-phonon interaction (i.e., a large $\dot{\gamma}^*_{e-p}$)[18], and a tunable bandgap (through functionalization[19]), make it a suitable candidate. Part II[20] tunes its bandgap to resonate with the optical phonon energy through hydrogenation (graphame)[21–23]. We find that the hydrogenation and the resulting shift from π to σ-bonding degrades the electron-phonon coupling, such that hot optical phonons primarily downconvert into acoustic phonons rather than generate electrons. However, the methodology for tuning and investigating a pV material is developed. Though the search for a new material upon which to apply the theory developed within this study is challenging, the potential benefits are shown to be substantial.

Part I of this study describes the pV cell. It examines the extent and limits of the pV regime and establishes the potential of the device to surpass the TE efficiency. First, a brief comparison with the TE and PV cells illustrates the unique features of the pV cell, the importance of nonequilibria, and the resulting nanoscale requirement (Section II). Then the central mechanisms of the pV cell, i.e., the electron-phonon and the anharmonic three-phonon coupling, are discussed (Section III). Next, the Boltzmann transport equation (BTE) and its solution via the Monte Carlo simulations illustrate the operation of a pV cell (Section IV). An analytical model is developed using the diode equation, a derived net-generation equation, and the resulting heat flow (Section V). Finally, a self-consistent hydrodynamic model incorporating two phonon temperatures validates the analytic model, illuminates additional conditions required for efficient pV operation, and shows that a high Z_{pV} pV outperforms a TE cell (Section VI). However, finding a suitable material remains very challenging.

II. ON THERMOELECTRICS AND PHONOVOLTAICS

In a TE cell, electrons diffuse down a temperature gradient, form the Seebeck potential, and absorb Peltier heat as they ascend a potential barrier at the semiconductor-metal junction. Simultaneously, heat conducts down the temperature gradient and generates entropy. Despite this, the efficiency grows with the spatial nonequilibrium across the cell, i.e., the Carnot efficiency (η_C). The TE figure of merit, Z_{TE}, and efficiency, η_{TE}, are

$$Z_{TE} = \frac{S^2 \sigma}{\kappa}, \quad \eta_{TE} = \eta_C \frac{(Z_{TE}T + 1)^{1/2} - 1}{(Z_{TE}T + 1)^{1/2} + 1 - \eta_C}, \quad \eta_C = \frac{T_h - T_c}{T_h}, \tag{3}$$

4

where S, σ, and $\kappa = \kappa_e + \kappa_p$ are the Seebeck coefficient and combined electrical and thermal conductivity, and T_c and T_h are the temperature at the cold and hot junctions of the TE cell (assuming $T_e = T_p$)[1,24]. Importantly, the local thermal equilibrium between the electron and phonon populations in a TE ensures coupled electric and thermal transport (e.g., through the Weidemann-Franz law) and limits Z_{TE}, such that $Z_{\mathrm{TE}}T > 1$ and $\eta_{\mathrm{TE}} > 0.2\eta_{\mathrm{C}}$ remain challenging to significantly surpass in paired p and n-type TE legs.

TABLE I. A comparison of thermoelectric (TE), phonovoltaic (pV), and photovoltaic (PV) cells and their controlling processes, where $j_e - \Delta\varphi$ is the current-voltage curve, and other symbols are defined in the text.

Property	TE[1]	pV	PV[25,26]
	Construction		
Size	μm to cm[5]	nm	nm to mm
Junction	p-metal-n	p-n	p-n
	Processes		
Energy Source	Heat	Optical Phonon	Photon
Power Generation	Diffusion	Generation	Generation
Entropy Generation	Conduction	Downconversion, $E_{p,\mathrm{O}} > \Delta E_{e,g}$	$E_{ph} > \Delta E_{e,g}$
nonequilibrium	Spatial	Local: Hot phonon	Local: Hot photon
	Performance		
$j_e - \Delta\varphi$	Linear	Exponential	Exponential
Figure of Merit	$S^2 T\sigma/\kappa$[24]	$\dot{\gamma}^*_{e-p}\Delta E_{e,g}/E_{p,\mathrm{O}}$	–
Quantum Efficiency	-	$\dot{\gamma}^*_{e-p}$	$(E_{ph} < \Delta E_{e,g})/E_{ph}$
Efficiency	Eq. (3)[24]	$F_F\eta_{\mathrm{C}}\dot{\gamma}^*_{e-p}\Delta E_{e,g}/E_{p,\mathrm{O}}$	$F_F\eta_{\mathrm{QE}}\Delta E_{e,g}/E_{ph}$[27]

Table I compares the pV cell to TE and PV cells, where F_F is the fill factor, and E_{ph} is the photon energy. While the TE and pV cells both harvest thermal energy, the pV is more similar to the PV cell, as both harvest a nonequilibrium population in a p-n junction. The major differences arise from the downconversion of optical phonons in a pV, and the transmission of photons with $E_{ph} < \Delta E_{e,g}$ in a PV cell. However, as the local nonequilibrium in a pV vanishes, so does the similarity between pV and PV cells. Instead, as the spatial, thermal nonequilibrium grows larger than the local nonequilibrium, the pV cell becomes more similar to a TV (or TE) cell.

That is, while the generation drives cell operation, the generated carriers replace, at most, those diffusing down the temperature gradient. Moreover, despite initially absorbing a single phonon per pair ($E_{p,\mathrm{O}}$), the generated electrons relax to a state of thermodynamic equilibrium, and the net energy required is given by the Peltier heat (ST). Finally, heat

conduction rather than downconversion drives entropy generation and the efficiency limit approaches that of a TE cell, i.e., Eq. (3). When a heat flux is applied to a pV cell, the local nonequilibrium drives up- rather than downconversion, and the conduction of that heat flux dominates entropy generation, such that the pV cell is limited by the TE efficiency and achieves this limit when the local nonequilibrium vanishes. Thus, a pV cell without a hot optical phonon population is a TV, which behaves like a TE. Here, the focus is on the pV regime, where the phonovoltaic behaves like a photovoltaic.

The pV regime requires that a direct excitation of the optical phonon population creates a large, local (rather than spatial) nonequilibrium in the pV cell. Let δ_{e-p} be the electron-phonon cooling length, such that $T_{p,\mathrm{O}} - T_e \simeq (T_{p,\mathrm{O}} - T_c) \exp(-L/\delta_{e-p})$ (the cooling length is on the order 100 nm in a typical semiconductor)[4]. Thus, $\eta_{\mathrm{pV}}/\eta_{\mathrm{C}} = \dot{\gamma}^*_{e-p} \exp(-L/\delta_{e-p})$ and achieving the maximum pV efficiency requires $L/\delta_{e-p} \lll 1$. However, the loss of local nonequilibrium compensated by the growth of the spatial nonequilibrium, which drives the thermoelectric effects. Thus, the TE efficiency replaces the pV efficiency as L/δ_{e-p} grows, such that $L/\delta_{e-p} = 1$ demarcates a qualitative boundary between the TE and pV regimes.

An efficient pV cell additionally requires $\dot{\gamma}^*_{e-p} > 0.5$, as small $\dot{\gamma}^*_{e-p}$ precludes efficient pV operation. Moreover, small $\dot{\gamma}^*_{e-p}$ indicates that the phonon-phonon nonequilibrium vanishes before the electron-phonon nonequilibrium, such that the pV cell achieves the TE limit most quickly as $\dot{\gamma}^*_{e-p} \to 1$. Thus, the third, conduction hindered (CH) region is defined by the $\dot{\gamma}^*_{e-p} \to 0$ and the $L/\delta_{e-p} \to 0$, where the downconversion of optical into acoustic phonons dominates energy conversion, generating entropy rather than power.

It is beyond the scope of this investigation to present the quantitative TV and CH regimes. However, Fig. 2 qualitatively illustrates the three regimes: The pV regime, where a hot optical phonon population relaxes primarily by generating electrons $[\eta^*_{\mathrm{pV}} = \dot{\gamma}^*_{e-p} \exp(L/\delta_{e-p}) > 0.5]$; the TV regime, where the local nonequilibrium vanishes $[\eta^*_{\mathrm{TE}} \approx 1 - \exp(\dot{\gamma}^*_{e-p} L/\delta_{e-p}) > 0.9]$; and the conduction hindered (CH) regime, where generation cannot supply the TE current (limiting the TV regime) or is dominated by downconversion (limiting the pV regime) $[1 - \eta^*_{\mathrm{pV}} - \eta^*_{\mathrm{TE}} = \exp(\dot{\gamma}^*_{e-p} L/\delta_{e-p}) - \dot{\gamma}^*_{e-p} \exp(L/\delta_{e-p}) > 0.7]$. Note that these contours have been chosen following the preceding discussion and for a pV cell which operates most efficiently in the pV rather than TE regime.
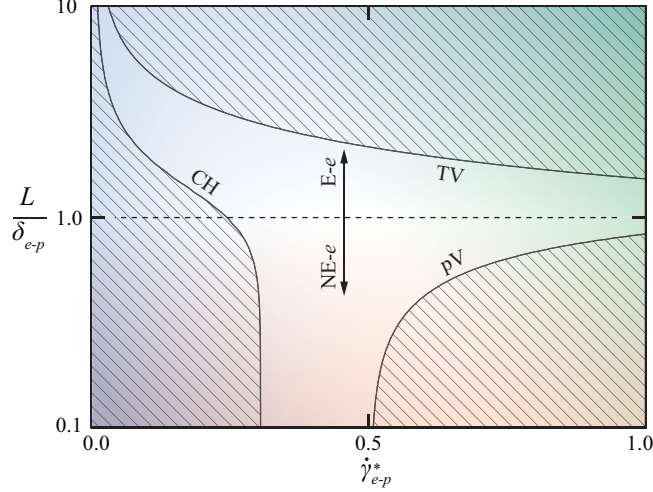
6

FIG. 2. Qualitative regimes of a pV cell for variations in L/δ_{e-p} and $\dot{\gamma}_{e-p}^*$. The pV regime requires (*i*) a device smaller than the electron-phonon cooling length, δ_{e-p}, to sustain a nonequilibrium between the optical phonon and electron populations (NE-*e*), and (*ii*) that generation dominates downconversion ($\dot{\gamma}_{e-p}^* > 0.5$). When the local nonequilibrium vanishes (E-*e*), the pV cell behaves as a TE (TV regime). When generation is much slower than downconversion ($\dot{\gamma}_{e-p}^* < 0.5$), conduction hinders or dominates the device operation (CH regime).

III.   ELECTRON-PHONON AND PHONON-PHONON COUPLINGS

As discussed, the fraction of hot optical phonons which relax by generating electrons rather than acoustic phonons ($\dot{\gamma}_{e-p}^*$) largely determines the performance of a pV cell. The electron-phonon (*e-p*) and anharmonic phonon (*p-p*) couplings drive these phenomena. This section presents the *ab initio* approach to the couplings and their kinetics from perturbation theory, as used in Part II[20].

A.   Electron generation

As a phonon displaces the atoms in a crystal, it shifts the potential field experienced by the electrons, and thus interacts with them. For a strong electron-phonon coupling, the displaced atoms must substantially affect the most energetic occupied electron states. For example, through the displacement of a linear chain of atoms, the bound electron state is distorted as the interatomic distance changes. However, for a scattering event to occur, not

only must phonon couple strongly to the bound state, but the resulting state must overlap significantly with an unbound, conduction state, and the scattering even must conserve momentum and energy. This is illustrated in Fig. 3.
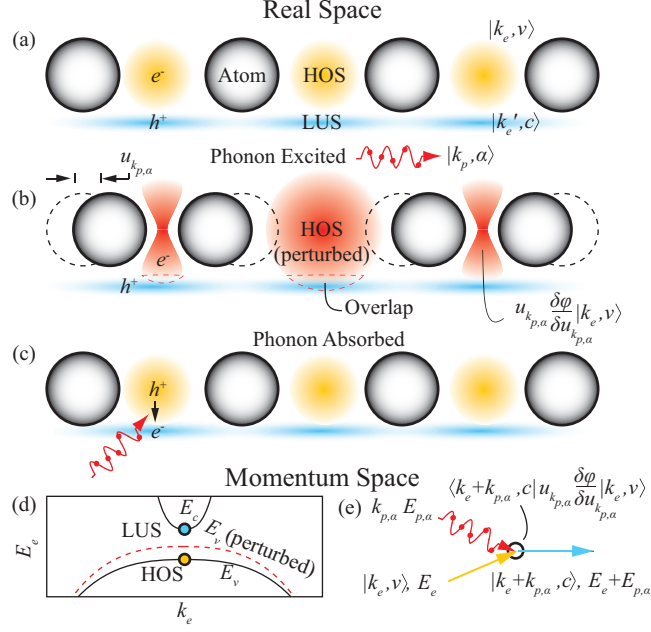

FIG. 3. The electron-phonon coupling during phonon absorption. (a) The unperturbed system is in equilibrium with an electron in the highest occupied state (HOS, $|\boldsymbol{k}_e, v\rangle$) and no electron in the lowest unoccupied state (LUS, $|\boldsymbol{k}_e', c\rangle$). (b) A phonon is excited ($\boldsymbol{k}_p, \alpha$), which displaces the atoms by $\boldsymbol{u}_{\boldsymbol{k}_{p,\alpha}}$ and perturbs the HOS, such that it overlaps with the LUS. (c) The electron in the perturbed HOS and excited phonon are annihilated and an electron is created in the highest occupied state, as shown in (c) $\boldsymbol{k}_e$ space and in (d) the Feynman diagram.

Perturbation theory provides the quantitative description of this qualitative illustration, where the Hamiltonian (H) is

$$H = H^\circ + H_{e-p} = H^\circ + \sum_{\boldsymbol{k}_e} \sum_{\boldsymbol{k}_{p,\alpha}} \frac{1}{2} \left(\frac{\hbar}{2\omega_{\boldsymbol{k}_{p,\alpha}}\langle m\rangle}\right)^{1/2} \frac{\partial\varphi}{\partial\boldsymbol{u}_{\boldsymbol{k}_{p,\alpha}}} (c^\dagger_{\boldsymbol{k}_e+\boldsymbol{k}_p} c_{\boldsymbol{k}_e} a_{\boldsymbol{k}_{p,\alpha}} + h.c.), \qquad (4)$$

where H° is the ground state energy the electron system and φ is the Kohn sham potential within density functional theory[28]. The factor of $1/2$ accounts for spin degeneracy, and the next term represents the displacement caused by a single phonon with wavevector $\boldsymbol{k}_p$, polarization α, frequency ω, moving atoms of average mass $\langle m\rangle$. This, times the derivative in potential with respect to the atomic displacement ($\boldsymbol{u}_{\boldsymbol{k}_{p,\alpha}}$) is the linear expansion of the

8

electron-phonon interaction potential. The final term describes the phonon-absorption and phonon-emission (the Hermetian conjugate, or $h.c.$) processes, where $c_{\boldsymbol{k}_e}$ $(a_{\boldsymbol{k}_p})$ and $c^{\dagger}_{\boldsymbol{k}_e}$ $(a^{\dagger}_{\boldsymbol{k}_p,\alpha})$ are the annihilation and creation operators for an electron (phonon) with momentum $\boldsymbol{k}_e$ $(\boldsymbol{k}_p$ and polarization α).

From the Fermi golden rule, the interaction rate depends on the perturbing Hamiltonian (e.g., H_{e-p}) operating on the initial state and overlap of this perturbed state with the final state. That is, the interaction element is[28]

$$M_{ij}^{(e\pm p,\alpha)}(\boldsymbol{k}_e, \boldsymbol{k}_p) = \frac{\hbar}{2\omega_{\boldsymbol{k}_p,\alpha}\langle m\rangle})^{1/2}\langle \boldsymbol{k}_e \pm \boldsymbol{k}_p, j|\frac{\partial \varphi}{\partial u_{\boldsymbol{k}_p,\alpha}}|\boldsymbol{k}_e, i\rangle, \tag{5}$$

where the positive sign corresponds to the absorption and the negative to the emission of a phonon, and the scattering rate is

$$\dot{\gamma}_{ij}^{(e\pm p,\alpha)}(\boldsymbol{k}_e, \boldsymbol{k}_p) = \frac{2\pi}{\hbar}|M_{ij}^{(e\pm p,\alpha)}(\boldsymbol{k}_e, \boldsymbol{k}_p)|^2 \times \delta(E_{e,i,\boldsymbol{k}_e} - E_{e,j,\boldsymbol{k}_e+\boldsymbol{k}_p} \pm \hbar\omega_{\boldsymbol{k}_p,\alpha})$$
$$\times f_{e,i,\boldsymbol{k}_e}(1 - f_{e,j,\boldsymbol{k}_e+\boldsymbol{k}_p})(\frac{1}{2} \mp \frac{1}{2} + f_{p,\alpha,\boldsymbol{k}_p}), \tag{6}$$

where $E_{e,i,\boldsymbol{k}_e}$ and $f_{e,i,\boldsymbol{k}_e}$ are the energy and population of an electron in band i with momentum $\boldsymbol{k}_e$ and $f_{p,\alpha,\boldsymbol{k}_p}$ is the phonon population.

The electron population terms ensure that scattering does not occur between two occupied states or two unoccupied states, such that scattering only occurs between an occupied and unoccupied state separated by the phonon energy ($\hbar\omega_{\boldsymbol{k}_p,\alpha}$). Thus, scattering is restricted to the valence states and conduction states ($i, j = v, c$) and dominated by interband interactions ($i \neq j$). Moreover, when $\Delta E_{e,g} > E_{p,\mathrm{O}}$, the scattering rate vanishes unless intraband ($i = j$) interactions contribute substantially, i.e., when the Fermi surface is within $k_{\mathrm{B}}T$ of the conduction or valence bands and $E_{p,\mathrm{O}} \gg k_{\mathrm{B}}T$. This is rare in a typical semiconductor, unless it is subjected to an exceptional doping intensity (becoming semi-metalic). Thus, the electron-phonon interaction typically contributes to the phonon linewidth only in semimetals and metals. In Part II, a semiconductor is sought with $E_{p,\mathrm{O}} \simeq \Delta E_{e,g} \gg k_{\mathrm{B}}T$ in order to overcome this tendency[20]. Otherwise, the phonon-phonon coupling described in the following section dominates the linewidth and $\dot{\gamma}^*_{e-p}$ vanishes.

However, finding or creating a material with a sufficiently energetic optical phonon and tuning to its bandgap to that phonon energy, $E_{p,\mathrm{O}} \simeq \Delta E_{e,g} \gg k_{\mathrm{B}}T$, is not sufficient. An efficient pV also requires a strong intraband coupling, i.e., that the lowest unoccupied states (LUS) and highest unoccupied states (HOS) overlap significantly, and that the optical

phonon perturbs these states substantially, as shown in Fig. 3 and described in Eq. (5). Thus, developing a pV material is very challenging.

For example, the tuned graphene structure investigated in Part II[20] achieves $E_{p,\mathrm{O}} \simeq \Delta E_{e,g} \gg k_\mathrm{B}T$, but exhibits hindered electron-phonon coupling. While the electron-phonon coupling dominates the optical phonon linewidth in graphene, hydrogenation transforms the π-bonds to σ-type bonds and reduces the overlap between the LUS and HOS. As its phonon-phonon coupling remains strong, any hot optical phonon population excited in hydrogenated graphene will primarily down-convert into acoustic phonons. This competing, phonon-phonon coupling is discussed next.

B. Optical phonon downconversion

The crystal Hamiltonian determines the phonon dynamics and the phonon-phonon couplings, and it is[26,29]

$$\langle \varphi \rangle = \langle \varphi \rangle_\circ + \frac{1}{2!} \sum_{ijxy} \Gamma_{ij}^{xy} d_i^x d_j^y + \frac{1}{3!} \sum_{ijkxyz} \Psi_{ijk}^{xyz} d_i^x d_j^y d_k^z + ..., \tag{7}$$

where $\langle \varphi_o \rangle$ is the equilibrium crystal potential, d_i^x is the displacement from equilibrium of atom i in the x (Cartesian) coordinate, and Γ_{ij} and Ψ_{ijk} are the second and third-order force constants.

The second-order interaction determines the phonon dynamics, i.e., the phonon frequencies ($\omega_{\boldsymbol{k}_p,\alpha}$) and eigenvectors ($\epsilon_{\boldsymbol{k}_p,\alpha}$), while the anharmonic (third-order and higher) interactions are responsible for the up and downconversion of phonons, the thermal expansion of the lattice, and the temperature dependence of the phonon frequencies. As the pV cell prefers slow downconversion, i.e., low anharmonicity, materials with small thermal expansion, etc., are desired.

Typically, the fourth-order and higher interactions are masked by the third-order coupling[30]. From the Fermi golden rule, the rate at which a phonon ($|\boldsymbol{k}_p, \alpha\rangle$) downconverts into two phonons ($|\boldsymbol{k}_p', \alpha'\rangle$ and $|\boldsymbol{k}_p'', \alpha''\rangle$)[31] is

$$\dot{\gamma}_{p-p}(\boldsymbol{k}_p, \alpha) = \frac{1}{N_{\boldsymbol{k}_p'}} \sum_{\alpha'\alpha''\boldsymbol{k}_p'\boldsymbol{k}_p''} \frac{\hbar\pi}{16} |\Psi_{\alpha\alpha'\alpha''}^{\boldsymbol{k}_p\boldsymbol{k}_p'\boldsymbol{k}_p''}|^2 \delta_{\boldsymbol{k}_p\boldsymbol{k}_p'\boldsymbol{k}_p''} \delta(\omega_{\boldsymbol{k}_p,\alpha} - \omega_{\boldsymbol{k}_p',\alpha'} - \omega_{\boldsymbol{k}_p'',\alpha''})(f_p' + f_p'' + 1),$$

$$\tag{8}$$

where f_p is the phonon occupancy, and the interaction element $\Psi_{\alpha\alpha'\alpha''}^{\boldsymbol{k}_p\boldsymbol{k}_p'\boldsymbol{k}_p''}$ is

$$\Psi_{\alpha\alpha'\alpha''}^{\boldsymbol{k}_p\boldsymbol{k}_p'\boldsymbol{k}_p''} = \sum_{ijk}\sum_{xyz}\Psi_{ijk}^{xyz}u_{\boldsymbol{k}_p,\alpha}^{xi}u_{\boldsymbol{k}_{p'},\alpha''}^{yj}u_{\boldsymbol{k}_{p'},\alpha''}^{zk}\exp(\boldsymbol{k}_p\cdot\boldsymbol{r}_i + \boldsymbol{k}_p'\cdot\boldsymbol{r}_j + \boldsymbol{k}_p''\cdot\boldsymbol{r}_k), \quad (9)$$

and $\boldsymbol{r}_i$ is the location of atom i. Here, $u_{\boldsymbol{k}_p,\alpha}^{xi}$ is proportional to the displacement of atom i in the x direction caused by the phonon $|\boldsymbol{k}_p,\alpha\rangle$, i.e.,

$$u_{\boldsymbol{k}_p,\alpha}^{xi} = \frac{\epsilon_{\boldsymbol{k}_p,\alpha}^{xi}}{(M_i\omega_{\boldsymbol{k}_p,\alpha})^{1/2}}. \quad (10)$$

Unlike the electron-phonon coupling, which decreases with temperature (due to the Fermionic electrons blocking scattering), the phonon-phonon couplings increase the hotter the acoustic phonon populations become (due to the Bosonic phonons enhancing scattering). This, among other factors, tends to push the pV cell towards low temperature operation. However, for an energetic optical phonon, the scattering rate only increases substantially at high temperature.

C.   Evaluating $\dot{\gamma}_{e-p}$, $\dot{\gamma}_{p-p}$, and $\dot{\gamma}_{e-p}^*$

The fraction of hot optical phonons which relax by generating an electron rather than a pair of acoustic phonons ($\dot{\gamma}_{e-p}^*$) follows from the electron-phonon and phonon-phonon scattering rates [Eqs. (6) and (8)]. While Eq. (8) gives the rate at which an optical phonon mode with $\boldsymbol{k}_p = \boldsymbol{0}$ and α ($f_{p,\mathrm{O}} = 1$) downconverts, Eq. (6) provides only the rate at which that optical phonon mode generates an electron with momentum $\boldsymbol{k}_e$ in band j. However, after summation over $\boldsymbol{k}_e$ for $i, j \in c, v$, Eq. (6) gives the rate of recombination or generation driven by that optical phonon mode, such that the net generation $\dot{n}_e$ is

$$\dot{n}_e(\boldsymbol{k}_p = \Gamma, \alpha) = \sum_{\boldsymbol{k}_e}[\dot{\gamma}_{cv}^{(e+p,\alpha)}(\boldsymbol{k}_e, \boldsymbol{k}_p = \boldsymbol{0}) - \dot{\gamma}_{vc}^{(e-p,\alpha)}(\boldsymbol{k}_e, \boldsymbol{k}_p = \boldsymbol{0})]. \quad (11)$$

$\dot{\gamma}_{e-p}^*$ follows

$$\dot{\gamma}_{e-p}^*(\Gamma, \alpha) = \frac{\dot{n}_e(\Gamma, \alpha)}{\dot{n}_e(\Gamma, \alpha) + \dot{\gamma}_{p-p}(\Gamma, \alpha)} = \frac{\dot{n}_e(\Gamma, \alpha)}{\dot{n}_e(\Gamma, \alpha) + \dot{n}_a(\Gamma, \alpha)}, \quad (12)$$

where $\dot{n}_a$ is the net rate of acoustic phonon-pair generation. This quantity limits the quantum efficiency of the pV, i.e., the number of electrons extracted for each optical phonon excited, as discussed in Section V.

In Part II, both the electron-phonon and phonon-phonon couplings for the Γ-point phonons ($\boldsymbol{k}_p = \boldsymbol{0}$) are evaluated within density functional perturbation theory (DFPT) using the *ab initio* Quantum Espresso code, which provides dynamical matrices, the electron-phonon matrix elements, and third-order force constants on a rough mesh of $\boldsymbol{k}_e$ and $\boldsymbol{k}_p$ points. Through the Fourier interpolation throughout the first Brillouin zone, the components required to evaluate Eqs. (6) and (8) are calculated on a fine mesh of $\boldsymbol{k}_e$ and $\boldsymbol{k}_p$ points. Then, the integrations are carried out (Part II[20] give the details).

IV. BOLTZMANN TRANSPORT

The nanoscale pV cell can exhibits several forms of nonequilibria. For example, the local nonequilibrium between electron and phonon populations drives the net generation of electrons, the local nonequilibrium between optical and acoustic phonon populations drives the net downconversion of optical phonons, and the local nonequilibrium within the electron system affects transport. Moreover, when the device is sufficiently long, a spatial nonequilibrium grows within these populations and the aforementioned local nonequilibria vanish. Thus, the investigation of a pV cell begins with the Boltzmann transport equation (BTE), which models spectral transport of an energy carrier (i) with momentum $\boldsymbol{p}$ through its occupancy $f_i(\boldsymbol{p})$. As such, it demonstrates the role of the electron-electron nonequilibrium and spatial nonequiblirium within a pV cell.

The electron BTE, $i = e$, is[26]

$$\frac{\partial f_e}{\partial t} + \boldsymbol{u}_e \cdot (\nabla_x f_e) + -e_c \nabla_x \varphi_e \cdot \nabla_p f_e = \frac{\partial f_e}{\partial t}|_s + \dot{s} \approx \dot{\gamma}_e(f_e - f_e^\circ) + \dot{s}_e, \qquad (13)$$

where the terms, in order, describes transient effects, the free flight of electrons with velocity $\boldsymbol{u}_e$, the acceleration by an electric field (where φ_e is the electric potential and e_c the electron charge), the in- and out-scattering of electrons at location $\boldsymbol{x}$, and the generation ($\dot{s}_e$) of new electrons with momentum $\boldsymbol{p}$. The scattering term is often approximated through the relaxation-time approximation (RTA), where f_e° is the equilibrium occupancy and $\dot{\gamma}_e$ is the total scattering rate. This approximation assumes that there is near equilibrium within the electron population, and it enables the integration of the BTE for various device level models.

Furthermore, the RTA provides the average distance between electron collisions (mean

free path), $\lambda_e = u_F/\langle\dot{\gamma}_e\rangle$, where u_F is the Fermi velocity and $\langle\dot{\gamma}_e\rangle$ is the average electron scattering rate. When the device is very small compared to the mean free path ($L \ll \lambda_e$), the transport is ballistic and generated electrons are harvested without relaxing. For $L \gg \lambda_e$, the transport is diffusive, electron distributions are near equilibrium ($f_e \simeq f_e^\circ$), and the RTA is valid. This section presents an ensemble Monte-Carlo (MC) simulation of the BTE in order to investigate the electron population in the active region of a pV cell and to describe the electron transport in a pV cell.

A. Ensemble Monte-Carlo simulations

The MC method statistically solves the BTE by simulating many electron superparticles freely-accelerating between electron-phonon scattering events. The time between scattering events and the scattering event which occurs are chosen statistically while preserving the kinetics of the system.[32]

Here, only the scattering of electron with the optical and acoustic phonon population is considered. Furthermore, the kinetics within the MC model assume isotropic, parabolic bands and a constant electron-phonon coupling element $[M_{cc}^{e-p,\alpha}(\boldsymbol{k}_e, \boldsymbol{k}_p) = M_{p,\alpha}]$ near the band-edge. Consider Eq. (6) integrated over $\boldsymbol{k}_p$ from the perspective of conduction electron with momentum $\boldsymbol{k}_e$ in a non-degenerate semiconductor ($f_{e,c,\boldsymbol{k}_e} = 1$ and $f_{e,c,\boldsymbol{k}_e\pm\boldsymbol{k}_e} = 0$). For a dispersionless optical phonon, this gives

$$\dot{\gamma}_{cc}^{(e\pm p,\mathrm{O})}(\boldsymbol{k}_e) = \sum_{\boldsymbol{k}_p} \dot{\gamma}_{cc}^{(e\pm p,\mathrm{O})}(\boldsymbol{k}_e, \boldsymbol{k}_p)$$
$$= \frac{2\pi}{\hbar}|M_{p,\mathrm{O}}|^2 D_e(E_{e,\boldsymbol{k}_e} \pm E_{p,\mathrm{O}})(\frac{1}{2} \mp \frac{1}{2} + f_{p,\mathrm{O}}), \tag{14}$$

where the density of states and electron dispersion are

$$D_e(E_e) = \sum_{\boldsymbol{k}_p} \delta_e(E_e) = (\frac{m_{e,e}}{\hbar^2})^{3/2} E_e^{1/2} \tag{15}$$

$$E_{e,\boldsymbol{k}_e} = \frac{\hbar^2|\boldsymbol{k}_e|^2}{2m_{e,e}}, \tag{16}$$

and $m_{e,e}$ is the effective mass of a conduction band electron.

The scattering rate of an electron with an acoustic phonon of constant speed $u_{p,\mathrm{A}}$ gives a similar result, only with a different phonon energy ($E_{p,\mathrm{A}} = \hbar|\boldsymbol{k}_p|u_{p,\mathrm{A}}$ rather than $E_{p,\mathrm{O}}$).

13

This energy must conserve energy and momentum, i.e., we require

$$E_{e,\boldsymbol{k_e}+\boldsymbol{k_p}} = E_{e,\boldsymbol{k_e}} \pm E_{p,\mathrm{A}}$$
$$\frac{\hbar^2(k_e+k_p)^2}{2m_{e,e}} = \frac{\hbar^2 k_e^2}{2m_{e,e}} \pm u_{p,\mathrm{A}}\hbar k_p$$
$$\text{s.t.} \quad k_p = 2(\pm\frac{m_{e,e}u_{p,\mathrm{A}}}{\hbar} - k_e)$$
$$\text{and} \quad E_{p,\mathrm{A}} = 2u_{p,\mathrm{A}}(\pm k_e m_{e,e} u_{p,\mathrm{A}} - \hbar k_e), \tag{17}$$

where $k_i = |\boldsymbol{k_i}|$ and the $k_{p,\mathrm{A}} = 0$ solution does not represent a scattering event. The MC model does not treat the acoustic phonon scattering as elastic, but uses the above equations to determine the final state.

Additionally, a fast generation rate ($\dot{s}_e$) is prescribed in the active region and the energetic optical phonon is given a hot temperature ($T_{p,\mathrm{O},h}$). The remaining optical and acoustic phonon modes are given a cold temperature equal to the contact temperature, T_c.

As ensemble MC simulates thousands of electrons in one superparticle, less than one superparticles is typically generated or annihilated within a single time step (1 fs) in a particular location bin (0.5 nm). This MC model carries the remainder from one time step to the next, such that over many time steps the number of generated superparticles accurately represents the number of generated electrons. New electrons are given an initial energy through the implicit solution of

$$r \int\limits_0^\infty D_e(E_e)D_e(E_e - E_{p,\mathrm{O}})\mathrm{d}E_e = \int\limits_0^{E_e} D_e(E_e - E_{p,\mathrm{O}})\mathrm{d}E_e, \tag{18}$$

for E_e, where r is a uniformly distributed random number and $D_e(E_e)D_e(E_e - E_{p,\mathrm{O}})$ is proportional to the net-generation rate. (See Section V.A.) The initial momentum direction is randomized in the isotropic semiconductor. A typical Ohmic contact is modeled at $x = 0$, and electrons are reflected at $x = L/2$, where L is the length of the cell, to represent an ideal junction under short-circuit conditions. This is illustrated in Fig. 4.

The simulations are run for the material parameters listed in Table II. These parameters are similar to those of the partially-hydrogenated graphite[20]. Note that the generation rate is proportional to the cell length. This ensures that in a long cell with $L \gg \lambda_e$, i.e., the diffusive regime, the change in the carrier concentration is independent of L. This simulation does not accurately track or predict the cell performance, as it is not self-consistent. However,

14

TABLE II. Material and parameters used in the MC simulations, where m_e is the electron mass. Parameters are chosen to represent partially-hydrogenated graphite.

MC Parameters			
$m_{e,e}$	0.01 m_e	$\Delta E_{e,g}$	150 meV
$E_{p,O,1}$	198 meV	$E_{p,O,2}$	154 meV
$|M_{p,O}|_1$	140 meV	$|M_{p,O}|_2$	110 meV
$u_{p,A}$	1000 m/s	$|M_{p,A}|$	50 meV
L_a	$1/5L$	$\dot{s}_e$	$0.1/L$ nm-cm^{-3}ps^{-1}
T_c	300 K	$T_{p,O,h}$	600 K

it determines the extent of the electron relaxation and the transport regime (ballistic or diffusive) for the generated electrons as a function of L. Most importantly, it illustrates the operation of a pV cell.

B. Results

Figure 4 shows the spatial distribution of the (a) electron density and (b) temperature and (c) the local distribution electron energy for variations in the cell length. Electrons are generated within a small active region near the junction. The junction reflects all electrons, forcing electrons towards collection at the contact. Note the concentration gradient formed in the short cell is half of that formed in the long cell. Indeed, the concentration gradient required to drive the generated electrons out of the cell is reduced as L approaches λ_e and the transport regime becomes ballistic.

Additionally, as these electrons have a smaller kinetic energy than the thermal average, $3k_B T_c/2$, they cool the cell. However, the hot optical phonon population also heats the electron population through intraband interactions. In the short cell, the cooling effect dominates, while in the long cell, the two effects balance. In sufficiently long cell, intraband interactions should overcome the cooling and induce a spatial non-equilibrium. Regardless, the electron population in both the 40 and 400 nm cells remains near the equilibrium distribution. Indeed, the RTA remains valid, even as the electron transport becomes ballistic.

In the following sections, macroscale models use the RTA to take moments of the electron BTE. While the MC results support this approach, there are restrictions to its validity. Primarily, at lower temperatures the mean free path grows substantially. Moreover, under an applied voltage, a significant number of electrons flow over the junction, gain a large kinetic
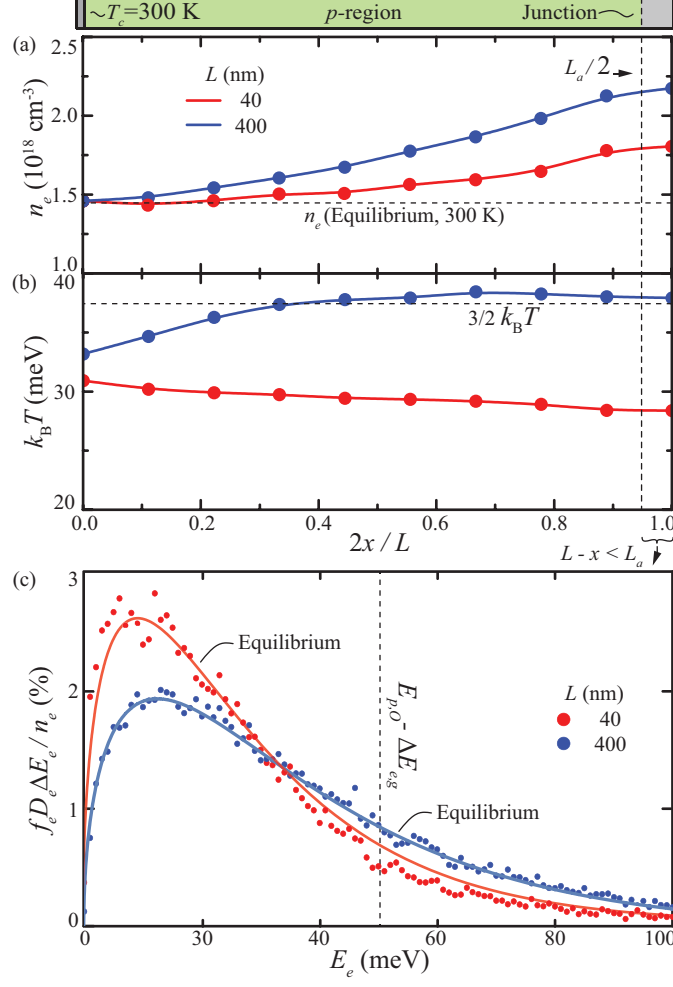
FIG. 4. Spatial distributions of the (a) Electron density and (b) temperature, and (c) local energy distributions within the active region in 400 and 40 nm pV cells. The generation rates are scaled by $1/L$ to demonstrate that transport is partially ballistic in the 40 nm cell. The generation of cold electrons reduces the average energy of the population, but the nonequilibrium within the electron population remains small. The 400 nm cell, in comparison, exhibits diffusive transport, a negligible change in the electron temperature, and equilibrium occupancy within the electron population.

energy, and these hot electrons are in nonequilibrium with the cold electron population. However, the mean free path of these hot electrons is relatively short. In general, the RTA and the resulting moments of the BTE remain valid.

16

V. ANALYTIC EFFICIENCY AND FIGURE OF MERIT

With the local nonequilibria limited to the electron-phonon and optical-acoustic phonon populations, a simple analytical model is developed in order to achieve the following goals: (*i*) develop a figure of merit, (*ii*) determine the temperature dependence of the pV cell, and (*iii*) provide accurate predictions and fundamental insights.

The ratio of the power produced ($P_e = J_e \varphi_a$, where J_e is the current extracted across a potential φ_a) to the heat flow applied (Q_{in}) determines the pV efficiency ($\eta_{\text{pV}} = P_e/Q_{in}$). In an ideal junction (i.e., one with no excess current loss, e.g., that from surface recombination or junction tunneling) with negligible internal resistance, the current produced is proportional to the net-generation ($\dot{n}_e$) within the cell volume (V), i.e, $J_e = e_c \dot{n}_e V$. The energy flow required to produce this current is $Q_e = E_{p,\text{O}} J_e$. However, additional heat flows from the hot optical phonon population into the acoustic branches due to the net-downconversion rate ($\dot{n}_{p,\text{A}}$) within the cell volume, such that $Q_{p,\text{A}} = E_{p,\text{O}} \dot{n}_{p,\text{A}} V$. Assuming the interband electron-phonon and phonon-phonon interactions dominate the optical phonon lifetime, the controlling equations become

$$P_e = J_e \varphi_a = e_c \dot{n}_e V \varphi_a \tag{19}$$

$$Q_{in} = Q_e + Q_{p,\text{A}} = E_{p,\text{O}}(\dot{n}_e + \dot{n}_a) \tag{20}$$

$$\eta_{\text{pV}} = \frac{P_e}{Q_{in}} = \frac{e_c \varphi_a}{E_{p,\text{O}}} \frac{\dot{n}_e}{\dot{n}_e + \dot{n}_{p,\text{A}}}. \tag{21}$$

Thus, determining the efficiency and power output of a pV cell requires the relationship between the current (or net-generation) and voltage.

Before deriving a model for this relationship, consider the diode equation

$$J_e(\varphi_a) = J_o - J_d(\varphi_a), \tag{22}$$

where $J_o = J_e(0)$ is the short-circuit current and J_d is the dark, adverse current driven across the junction by a potential (or, alternatively, the net-recombination driven by the potential induced difference in electron and hole Fermi-levels). In an open-circuit, no current leaves the cell ($J_e = 0$). Instead, the potential develops within the cell until it reaches the open-circuit voltage ($\Delta \varphi_{oc}$) and the dark current balances with the short-circuit current generated by the hot optical phonon population.

Note that short-circuiting the pV cell ($\varphi_a = 0$) and maximizing the current, or open-circuiting the cell ($J_e = 0$) and maximizing the voltage generates no power. The maximum

power and maximum efficiency conditions reside between these limits. The fill-factor (F_F) quantifies the fraction of power achieved by a diode to the product of the short-circuit current and open-circuit voltage, i.e.,

$$F_F = \frac{P_e}{J_o \Delta \varphi_{oc}}. \tag{23}$$

The fill-factor is limited to between 1/4 and 1, where the former requires a linear current-voltage curve and the latter requires a square curve. Next, analytic equations for the current-voltage relationship of an ideal pV cell and the resulting performance are derived.

A.   Net generation

The electron-phonon interband interaction falls into the class of band-to-band recombination and generation events, which also includes radiative decay. A band-to-band recombination rate ($\dot{n}_{e,b-b}$) depends on the number of conduction electrons (n_e) which can recombine and the number of empty valence states, i.e., holes (n_h), with which they can recombine. Thus, the generation or recombination rate is expected to be proportional $n_e n_h$. Noting that no net recombination occurs under equilibrium, when $n_e n_h = n_i^2$ and n_i is the intrinsic electron and hole concentration. Thus, the net band-to-band recombination rate is

$$\dot{n}_{e,b-b} = a_{b-b}(n_e n_h - n_i^2), \tag{24}$$

where a_{b-b} is a coefficient which depends on the interaction. We show below that the net rate of generation due to the electron-phonon interaction exhibits a similar form when derived from the *ab initio* rate [Eq. (6)].

Consider Eq. (6), integrated over $\boldsymbol{k}_p$ for a dispersionless optical phonon ($\hbar\omega_{\boldsymbol{k}_p,O} = E_{p,O}$) with a constant interaction strength for generation [$M_g = M_{vc}^{(e+p,O)}(\boldsymbol{k}_e, \boldsymbol{k}_p)$] and recombination [$M_r = M_{cv}^{(e-p,O)}(\boldsymbol{k}_e, \boldsymbol{k}_p)$] events. Further, assume there is equilibrium within the electron, hole, and optical phonon populations and thermal equilibrium between the electron and hole populations. Finally, assume a non-degenerate semiconductor where Maxwellian statistics hold, i.e., the population of the the electron ($i = e$), hole ($i = h$) and phonon ($i = p$) are

$$f_i(E_i, T) = \exp(\frac{E_{F,i} - E_i}{k_B T}) \ll 1, \tag{25}$$

18

where E_i and T are the population energy and temperature, and $E_{\mathrm{F},i}$ is the Fermi energy ($E_{\mathrm{F,p}} = 0$).

Under these assumptions, the generation $[\dot{\gamma}_{e-p,g}(E_e)]$ and recombination $[\dot{\gamma}_{e-p,r}(E_e)]$ rates for an electron at initial energy E_e are

$$\dot{\gamma}_{e-p,g}(E_e) = a_{e-p,g} \int \mathrm{d}\boldsymbol{k}_p \delta_E(E_e - E_e' + E_{p,\mathrm{O}}) f_{p,\mathrm{O}}(E_{p,\mathrm{O}}, T_{p,\mathrm{O}})$$

$$\dot{\gamma}_{e-p,r}(E_e) = a_{e-p,r} \int \mathrm{d}\boldsymbol{k}_p \delta_E(E_e - E_e' - E_{p,\mathrm{O}}) f_e(E_i, T) f_h(E_f, T), \tag{26}$$

where $a_{e-p,i} = \pi\hbar|M_i|^2/(E_{p,\mathrm{O}}\langle m \rangle)$. Using the definition of the density of states, $D_i(E_i) = \int \mathrm{d}\boldsymbol{k}_p \delta_E(E_i)$, reduces the rates to

$$\dot{\gamma}_{e-p,g}(E_h) = a_{e-p,g} D_e(E_{f,h}) f_{p,\mathrm{O}}(E_{p,\mathrm{O}}, T_{p,\mathrm{O}})$$

$$\dot{\gamma}_{e-p,r}(E_e) = a_{e-p,r} D_h(E_{f,i}) f_{eh}(E_{p,\mathrm{O}}, T_{p,\mathrm{O}}), \tag{27}$$

where f_{eh} uses the differences in Fermi energy $E_{\mathrm{F},eh} = \Delta E_{\mathrm{F}} = E_{\mathrm{F},e} - E_{\mathrm{F},h}$, and $E_{f,i} = E_{p,\mathrm{O}} - \Delta E_{e,g} - E_i$.

Integrating over the allowed electronic states gives the total rate of generation ($\dot{n}_{e,g}$) and recombination ($\dot{n}_{e,r}$). Let $\mathscr{D}$ be the integral of $D_e(E_e)D_h(E_{f,e})$ over $0 \leq E_e \leq E_{p,\mathrm{O}} - \Delta E_{e,g}$ and $E_h = E_{p,\mathrm{O}} - \Delta E_{e,g} - E_e$, then the net rate of generation is

$$\dot{n}_e = \dot{n}_{e,g} - \dot{n}_{e,r} = a_{e-p,g}\mathscr{D} f_{p,\mathrm{O}}(E_{p,\mathrm{O}}, T_{p,\mathrm{O}}) - a_{e-p,r}\mathscr{D} f_{eh}(E_{p,\mathrm{O}}, T). \tag{28}$$

As the net generation must vanish under equilibrium ($T_{p,\mathrm{O}} = T$), we require $a_{e-p,g} = a_{e-p,r}$.

This model, like the band-to-band model, is driven by the temperature difference $T_{p,\mathrm{O}} - T$. However, the population terms $f_{p,\mathrm{O}}(E_{p,\mathrm{O}}, T_{p,\mathrm{O}}) - f_{eh}(E_{p,\mathrm{O}}, T)$ rely on $E_{p,\mathrm{O}}$ rather than $\Delta E_{e,g}$, as in the band-to-band model ($\dot{n}_{e,b-b}$), i.e.,

$$\dot{n}_{e,b-b} \propto [\exp(-\frac{\Delta E_{e,g}}{k_{\mathrm{B}}T_{p,\mathrm{O}}}) - \exp(-\frac{\Delta E_{e,g} - \Delta E_{\mathrm{F}}}{k_{\mathrm{B}}T})] \tag{29}$$

$$\dot{n}_e \propto [\exp(-\frac{E_{p,\mathrm{O}}}{k_{\mathrm{B}}T_{p,\mathrm{O}}}) - \exp(-\frac{E_{p,\mathrm{O}} - \Delta E_{\mathrm{F}}}{k_{\mathrm{B}}T})]. \tag{30}$$

This difference leads to a substantial divergence in the predicted behavior, and most notably, the open-circuit voltage. Noting that the $\Delta E_{\mathrm{F}} = e_c \varphi_a$ under the current assumptions, i.e., negligible internal resistance in an ideal junction, the open-circuit voltage $[\dot{n}_e(\Delta E_{\mathrm{F}} = e_c \Delta \varphi_{oc}) = 0]$ is

$$\Delta\varphi_{oc,b-b} = \eta_{\mathrm{C}}\Delta E_{e,g}/e_c \tag{31}$$

$$\Delta\varphi_{oc} = \eta_{\mathrm{C}}E_{p,\mathrm{O}}/e_c, \tag{32}$$

where $\eta_C = 1 - T/T_{p,O}$.

Typically, the open-circuit voltage in a photovoltaic cell is limited by the bandgap[33] rather than the photon energy. While it has been proposed that harvesting electrons before they relax enhances the open-circuit voltage[34], this has not been realized experimentally. In a pV cell, a similar phenomena is expected, where the relaxation of the generated carriers towards the bandedge ensures the same, bandgap-limited behavior. Therefore, the analytical model uses the band-to-band model for net-generation.

B. Current-voltage curve

As previously discussed, the current-voltage relationship is proportional to the net-generation, i.e.,

$$J_e(\varphi_a) = e_c V_a \dot{n}_e = e_c V_a a_{e-p,b-b}[\exp(-\frac{\Delta E_{e,g}}{k_B T_{p,O}}) - \exp(-\frac{\Delta E_{e,g} - \varphi_a}{k_B T})], \tag{33}$$

where $a_{e-p,b-b}$ ensures that the short-circuit band-to-band current matches the derived model in Eq. (28). The maximum power (P_m) and the corresponding voltage ($\Delta\varphi_m$) are found by maximizing $P_e(\varphi_a) = J_e(\varphi_a)\varphi_a$. The maximization gives

$$\Delta\varphi_m = \frac{k_B T}{e_c}\{W[\exp(1 + \frac{\Delta\varphi_{oc}}{k_B T})]\} \tag{34}$$

where $W(z)$ is the principle solution for w in $z = we^w$ and $\lim_{x\to\infty} W[\exp(1+x)] = x$. That is, as the open-circuit voltage grows large in comparison to $k_B T$, the $\Delta\varphi_m$ approaches the open-circuit voltage. Intuitively, this also implies the current (J_m) approaches the short-circuit current and the Fill-Factor approaches unity under the same condition. While the expressions for J_m and P_m becomes progressively more complicated and less insightful, numerical investigation confirms this. Indeed, the fill-factor expression corresponding to the maximized power condition is well approximated by

$$F_F = \frac{J_m \Delta\varphi_m}{J_o \Delta\varphi_{oc}} \simeq 1 - \frac{3}{4}\exp(-0.1\eta_C \Delta E_{e,g}^*) \text{ for } \eta_C \Delta E_{e,g}^* < 10, \tag{35}$$

where $\Delta E_{e,g}^* = \Delta E_{e,g}/k_B T$ and the limits $1/4 \leq F_F \leq 1$ are reproduced, and this equation confirms these suppositions.

C. Efficiency

From Eq. (31), the fraction of the optical phonon energy achieved by the pV cell in an open-circuit is

$$\eta_\varphi = \frac{e_c \Delta \varphi_{oc}}{E_{p,O}} = \eta_C \frac{\Delta E_{e,g}}{E_{p,O}}. \tag{36}$$

Additionally, the number of electrons extracted per optical phonon (quantum-efficiency) follows from Eqs. (20) and (33)

$$\eta_{QE} = \frac{J_o}{J_{p,O}} = \frac{e_c V_a \dot{n}_e}{e_c V_a (\dot{n}_e + \dot{n}_a)} = \frac{\dot{n}_e}{(\dot{n}_e + \dot{n}_a)} = \dot{\gamma}^*_{e-p}, \tag{37}$$

where $\dot{\gamma}^*_{e-p}$ is the fraction of optical phonon scattering events which result in the generation of an electron [from Eq. (12)]. Thus, the efficiency for a square current-voltage curve ($F_F = 1$) is

$$\eta_{pV,max} = \eta_C \dot{\gamma}^*_{e-p} \frac{\Delta E_{e,g}}{E_{p,O}} = \eta_C Z_{pV}, \tag{38}$$

where $Z_{pV} = \dot{\gamma}^*_{e-p} \Delta E_{e,g}/E_{p,O}$ is the pV figure of merit.

Unfortunately, the analytic expressions for the maximum efficiency condition is much more complicated than the already complex expressions for $\Delta \varphi_m$ and P_m. Thus, a realistic and maximized analytic efficiency offers little insight. However, consider the following conservative procedure to derive an analytic and insightful efficiency relation (η_{pV}).

The maximum heat flow required by a pV cell occurs in the short-circuit condition, where $\dot{n}_e$ is maximized. Assuming Q_{in} does not strongly depend on φ_a and remains near this limit, we can derive a useful relation. If Q_{in} does not depend on φ_a, then the maximum power and efficiency conditions coincide. Thus,

$$\eta_{pV} = \eta_C Z_{pV} F_F \simeq \eta_C Z_{pV} [1 - \frac{3}{4} \exp(-0.1 \eta_C \Delta E^*_{e,g})], \tag{39}$$

where F_F is approximated as in Eq. (35).

Assuming a constant Q_{in} presumes that either $\dot{\gamma}^*_{e-p} \to 0$ or $F_F \to 1$ ($\eta_C \Delta E^*_{e,g} \to 1$). For large $\dot{\gamma}^*_{e-p}$ and small F_F, the heat decreases quickly with increasing φ_a (and decreasing J_e). In this case, the maximum efficiency and power conditions diverge, and the maximum efficiency increases significantly over Eq. (39). A parameterized investigation of Eq. (39) and its implications follows, and in the next section we look at the divergence of this relation from the results of a relaxed, hydrodynamic model.
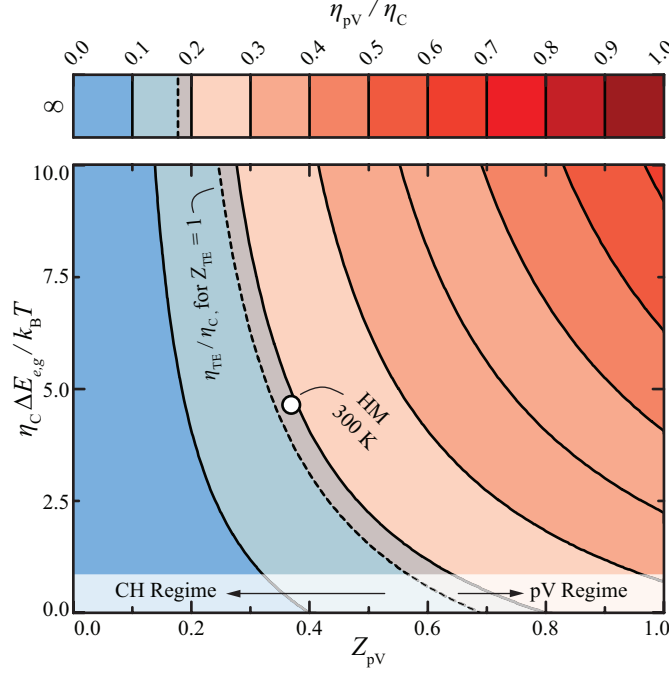
21

D. Results

FIG. 5. The pV efficiency as a function of the nonequilibrium, $\eta_C \Delta E_{e,g}/k_B T_c$, and the pV figure of merit, Z_{pV} [Eq. (39)]. Significant nonequilibrium is required to outperform a TE with $Z_{TE}T = 1$, unless the figure of merit exceeds 0.7. When T_c vanishes, the pV cell achieves $\eta_{pV} = \eta_C Z_{pV} \leq 1$. When $Z_{pV} \to 0$, the efficiency vanishes, and when $\eta_C \to 0$, the efficiency approaches $0.25\eta_C Z_{pV}$. The hydrodynamic model (HM) simulations use a standard set of parameters slightly exceeding the TE cell.

Figure 5 depicts Eq. (39), showing η_{pV}/η_C for variations in Z_{pV} and $\eta_C \Delta E_{e,g}^*$. In order to surpass η_{TE}, a pV must achieve $\eta_C \Delta E_{e,g}^* > 1$, unless $Z_{TE}T > 0.7$. Thus, an efficient pV cell requires either an optical phonon resonant with its bandgap and a linewidth dominated by the electron-phonon coupling, or it requires extreme nonequilibrium and a bandgap significantly more energetic than the thermal energy. That is, unless Z_{pV} is large, the pV is limited to low-temperature operation. However, if the Z_{pV} and nonequilibrium are large, the pV cell approaches the Carnot limit.

22

VI. HYDRODYNAMIC EFFICIENCY AND OPERATION

The analytical model requires a number of assumptions including fast transport and no surface recombination ($\eta_{QE} = \dot{\gamma}^*_{e-p}$). A numerical, hydrodynamic model (given in Appendix A) is used to validate Eq. (39), relax its assumptions, and reveal additional cell parameters which influence the pV efficiency. The hydrodynamic model considers the same nonequilibria as the analytic model, i.e., local e-p and p-p nonequilibria, but adds the spatial nonequilibria within electron and phonon populations. It takes the first three moments of the electron BTE (continuity, momentum, energy), includes the conduction of optical and acoustic phonons, and uses the Poisson equation to ensure self-consistency.

TABLE III. Material and parameters used in hydrodynamic model simulations at $T_c = 300$ K. Parameters are chosen to represent a hydrogenated graphite pV cell. Parameters are defined in Appendix A.

Figure of Merit			
$E_{p,\mathrm{O}}$	198 meV	$\Delta E_{e,g}$	150 meV
a_{e-p}	20 cm^{-9}s^{-1}	a_{p-p}	20 cm^{-9}s^{-1}
$\tau_{e-p,E}$	20 ps	$\Delta E_{e,g}/E_{p,\mathrm{O}}$	0.75
$\dot{\gamma}^*_{e-p}$	0.5	Z_{pV}	0.38
Transport			
$n_{e,v}$	7.1×10^{18} cm^{-3}	$n_{e,c}$	7.1×10^{18} cm^{-3}
μ_e	0.2 m^2/V-s	ϵ_e	12
$\kappa_{p,\mathrm{A}}$	0.3 W/m-K	$\kappa_{p,\mathrm{O}}$	0.001 W/m-K
Cell			
L	50 nm	L_a	10 nm
η_{C}	2/3	$\Delta E_{\mathrm{F},p-n}$	150 meV
SR	w/o		

This section uses the parameters baseline given in Table III, and then varies important parameters from among this collection to investigate their effects. The parameters are chosen to reflect a functionalized graphene material utilizing its $E_{2\mathrm{g}}$ optical phonon mode. The Z_{pV} is chosen to examine a moderate pV material which requires significant nonequilibrium to surpass a TE cell. Parameters a varied to both validate the analytic model, examine what is required for such a material to surpass the TE limit, and investigate pV cell operation under extreme nonequilibrium.

The length (L) is sufficiently small and the transport of the electron (μ_e), hole (μ_h), and acoustic phonon ($\kappa_{p,\mathrm{A}}$) are sufficiently fast to ensure that these population do not equilibrate with the optical phonon mode (limited spatial nonequilibrium). As long as this

23

condition is satisfied (i.e., $L \gg \delta_{p-p} \simeq \delta_{e-p}$, where δ_{e-p} is the electron cooling length), the pV behavior is independent of these parameters. However, the slow optical phonon transport ($\kappa_{p,\mathrm{O}}$) influences pV efficiency when $L_a/L < 1$, as it restricts the hot optical phonon population to the active region. In the standard cell, the active length (L_a), i.e., the region where the optical phonon population is excited, is restricted to the junction itself, which is approximately 10 nm, and the diode is doped such that the difference between the Fermi energy in the p and n regions ($\Delta E_{\mathrm{F},p-n}$) equals the bandgap. Finally, the surface recombination (SR) is inhibited, a requirement for efficient operation (Section VI B) and an assumption of the analytical model.

Note that the extent of the nonequilibrium, η_{C}, rather than the input heat or optical phonon temperature, is maintained at $\eta_{\mathrm{C}} = 2/3$. This enables a simplified comparison between the hydrodynamic and the analytical models, which predicts $\eta_{\mathrm{pV}} \propto \eta_{\mathrm{C}}$. This represents a substantial nonequilibrium state. Moreover, this leads to large current and heat densities. For example, at $T_c = 300$ K, the optical phonon is excited to 900 K, a short circuit current density of nearly 1000 A/mm^2 is generated, and a heat flux of 1000 W/mm^2 is required. To avoid such large fluxes, a smaller phonon linewidth, a high figure of merit or small nonequilibrium are required.

Figure 6 summarizes the hydrodynamic results for variations in the dimensionless bandgap ($\Delta E_{e,g}^* = \Delta E_{e,g}/k_{\mathrm{B}}T_c$) and the Carnot limit ($\eta_{\mathrm{C}}$: primarily influences the fill-factor and open-circuit voltage), the intrinsic diode potential ($\Delta E_{\mathrm{F},p-n}/e_c$: primarily affects the open-circuit voltage) and the active length (L_a: primarily affects pV operation at high temperatures). While $\dot{\gamma}_{e-p}^*$, $\Delta E_{e,g}/E_{p,\mathrm{O}}$, and Z_{pV} are constant in these pV cell, Fig. 9 (end of section) shows the pV efficiency for variations in these parameters and highlights the agreement between the analytical and hydrodynamic models when $\dot{\gamma}_{e-p}^* < 0.5$ and $L_a = L$. The analytical model gives a reasonable estimate across a wide range of parameters. However, there is significant discrepancy. This section explains the factors responsible for the difference and highlights the additional diode parameters required for effective pV operation.

A. Device operation

Before delving into the myriad parameters influencing the pV efficiency and its divergence from the analytical model, Fig. 7 illustrates the internal operation of the pV cell at 300
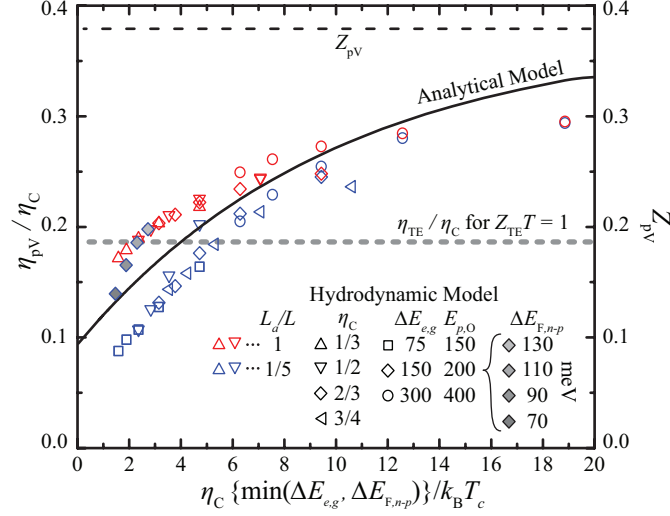
FIG. 6. The pV efficiency as a function of $\eta_C \Delta E_{e,g}^*$ for variations in $\Delta E_{e,g}^*$ and η_C. As shown, the analytical model [Eq. (39)] provides a reasonable estimate for the pV cell performance. A significant nonequilibrium ($\eta_C \Delta E_{e,g}^*$) is required to exceed the TE efficiency (shown for $Z_{TE}T = 1.0$) when $Z_{pV} < 0.7$.

K under the applied voltage which maximizes η_{pV} ($\Delta\varphi_a = 5$ mV). In this cell, the optical phonon is excited within the junction, driving generation. The electrons and holes are separated by the junction and transported to and collected by the contacts. The applied voltage simultaneously drives carriers across the junction, reducing the net generation of electrons within the active region and inducing their recombination outside of it. While downconversion primarily occurs within the active region, it extends throughout the entire cell. The analytic model, in comparison, assumes the hot optical phonon population diffuses throughout the entire volume ($L_a = L$), driving substantial downconversion and generation. This leads to a decrease in the open-circuit voltage and performance loss, as shown in Figs. 6 and 8. Note that the electron, hole, and acoustic phonon transport are sufficiently fast to ensure their respective population does not equilibrate with the optical phonon.

In Fig. 8, the (a) dimensionless and (b) dimensional current-voltage curves for this cell are shown for variations in the contact temperature. The dimensionless curves highlight the analytical limits, $\eta_{QE} = \dot{\gamma}_{e-p}^*$, and $\Delta\varphi_o = \eta_C \Delta E_{e,g}/e_c$, while the dimensional curves illustrate how a practical pV cell should behave. In particular, it depicts the efficiency loss at high temperatures, where the increased dark current reduces the fill-factor and the open-circuit voltage. While the short-circuit current vanishes with the temperature, the
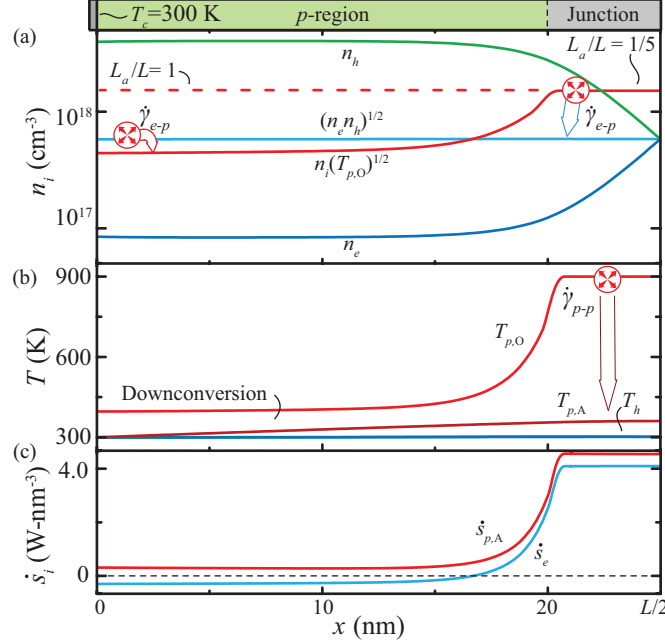
FIG. 7. Spatial distributions of (a) the electron and hole densities, (b) population temperatures, and (c) generation and downconversion rates for a pV cell under 5 mV of applied voltage (maximum power) with $T_c = 300$ K and $T_{p,O} = 900$ K in the active region. The abrupt drop in the optical phonon temperature outside the active region leads to recombination and a lowered open-circuit voltage. Downconversion, however, extends throughout the cell.

quantum efficiency remains constant. Indeed, low temperatures reduce both generation and downconversion rates, such that the current loss is balanced by the reduced downconversion rate. Additionally, the reduced relaxation rate in a cold cell enables the optical phonon to diffuse throughout the cell, despite its slow transport, and drive generation. Thus, the open-circuit voltage in a cold pv cell approaches that of a pV cell with $L_a = L$, i.e., that predicted by the analytical model. Furthermore, Fig. 8 shows that both the quantum efficiency and open-circuit voltage are significantly reduced when the surface recombination (SR) is not inhibited.

Furthermore, the dimensional curves in Fig. 8(b) emphasize the substantial current densities in a pV cell (and thus the heat density required to drive it). Three factors influence the current density: (i) the hot phonon temperature, $T_{p,O}$, (ii) the extent of the nonequilibrium, η_C, and (iii) the coupling strengths, a_{e-p} and a_{p-p}. Increasing these parameters increases the rate of hot optical phonon relaxation (heat required for a given η_C) and the electron pro-
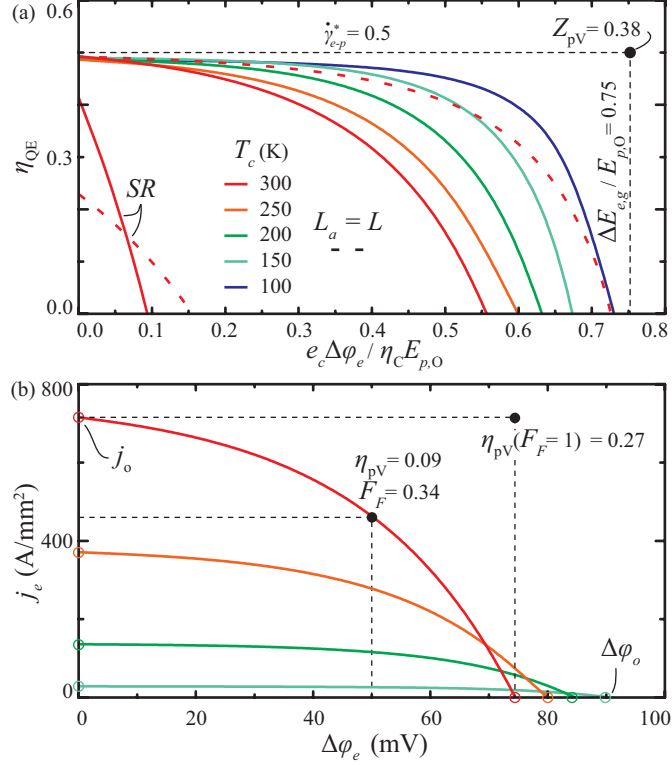
FIG. 8. (a) Dimensionless and (b) dimensional current-voltage curves for variations in T_c for the pV cell parameters in Table III. As expected, the quantum efficiency, open-circuit voltage ($\Delta\varphi_o$), and efficiency are limited by $\dot{\gamma}^*_{e-p}$, $\eta_C \Delta E_{e,g}$, and Z_{pV}. This limiting efficiency is approached as T_c vanishes and the nonequilibrium extends across the entire cell, i.e., when $F_F \to 1$ and $L_a = L$.

duction (j_e). Thus, if lower current densities are desired, a cold cell and an optical phonon weakly coupled to the electron and phonon systems are required. Additionally, restricting L_a reduces the current generated within the pV cell.

B. Achieving Analytic Efficiency

A myriad factors influence cell operation. In order to achieve the predictions offered by the analytic model, a few cell design factors are crucial, the most crucial of which are highlighted here in order of importance. (i) Electron transport and pV length must ensure the electron-phonon nonequilibrium persists. (ii) Surface recombination must be inhibited. (iii) There must be sufficient doping. (iv) The optical phonon must diffuse throughout the cell. Briefly, these four factors are discussed below.

27

The core concept of the pV cell requires that local electron-phonon nonequilibrium exists. If electron transport is exceptionally slow or the cell is sufficiently long (e.g., order of μm), a large concentration gradient forms between the active region and the contact. The excess electrons in the active region block generation and reduce the quantum efficiency.

Surface recombination decimates the pV efficieny, and it does so in two ways. First, the minority carriers generated near the contacts tend to diffuse into those contacts and recombine. These generation events only produce entropy and lower the quantum efficiency, as shown in Fig. 8. Second, the small size of the pV cell implies that minority carriers driven over the junction by an applied voltage tend to reach the contact. If their entrance is not inhibited,[35]

With no doping, no junction forms, minority and majority carriers are not separated, and the open-circuit voltage vanishes. Indeed, while the analytical model predicts that the open-circuit voltage is limited by the bandgap, it is truly limited by the change in the Fermi level from the p to n regions of the pV cell ($\Delta E_{\mathrm{F},p-n}$). Thus, to achieve the analytic prediction, the change in Fermi level must exceed $\eta_{\mathrm{C}}\Delta E_{e,g}$.

Less important, but noticeable, is the ratio of the active region to the total volume. While generation occurs only in the active region, the applied voltage tend to drive minority carriers throughout the entire pV cell, where they recombine. This in turn reduces the open-circuit voltage, as shown in Fig. 8. Note that the analyitcal model assumes $L_a/L = 1$, such that $L_a/L = 0.2$ leads to a slight underperformance. At higher temperatures, this is especially noticeable, as the optical phonons relax quickly and do not escape the active region. At low temperatures, the cooling length is much larger, such that the optical phonon diffuses throughout the pV cell, regardless of the active length.

C. Exceeding Analytic Efficiency

Just as a myriad factors reduce pV performance below that predicted by the analytic model, there are a few important factors that enhance pV cell operation. Primarily, these factors are slow acoustic phonon transport and large $\dot{\gamma}^*_{e-p}$. When acoustic transport is slow, the acoustic phonon population in the active region heats up significantly. This reduces the net rate of downconversion. When $\dot{\gamma}^*_{e-p}$ is large, the analytic model overpredicts the heat requirements.
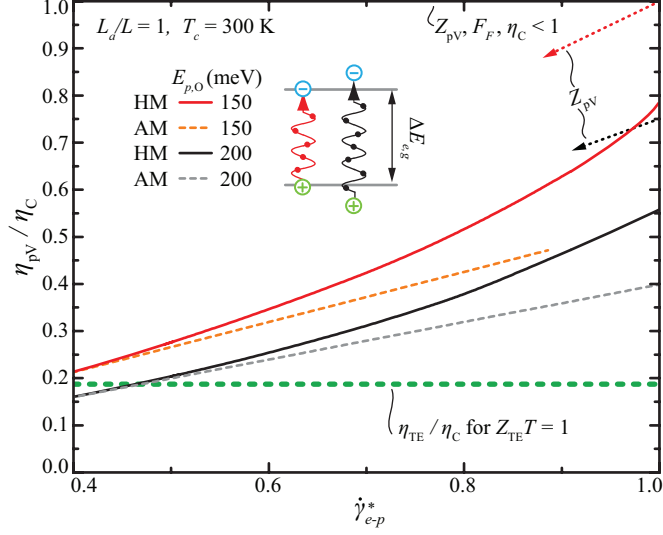
FIG. 9. Efficiency of a pV cell for variations in $\dot{\gamma}^*_{e-p}$ using the analytical (AM) and hydrodynamic (HM) models. While increased resonance between $E_{p,O}$ and $\Delta E_{e,g}$ increases efficiency, increasing $\dot{\gamma}^*_{e-p}$ enables the efficiency to approach its limit: $\eta_C Z_{pV}$. Moreover, it greatly reduces the impact the temperature has on the efficiency and enables efficient room-temperature operation. The TE efficiency is shown for comparison.

Consider a pV cell with a large $\dot{\gamma}^*_{e-p}$. In this case, the optical phonon relaxes solely through the production of electrons. At open-circuit conditions, no heat is required to maintain the hot optical phonon population.[36] The analytic model, conversely, predicts that the heat requirement does not change, even as the electron-phonon coupling slows. Thus, the analytic model greatly overestimates heat requirements when $\dot{\gamma}^*_{e-p}$ approaches unity and the fill-factor is small (i.e., when the net generation rate decreases quickly as the applied voltage grows).

In Fig. 9, this discrepancy is illustrated for a pV cell at room temperature (300 K). Moreover, these results are for a moderate fill-factor (around 0.7). When η_C vanishes, the current-voltage curve becomes linear. In this case, achieving a large $\dot{\gamma}^*_{e-p}$ ensures a significant reduction in the heat required to operate at maximum efficiency. Thus, the hydrodynamic simulations (HM) diverge from the analytical model (AM) for $\dot{\gamma}^*_{e-p} > 0.4$. Indeed, as $\dot{\gamma}^*_{e-p}$ aproaches unity, the pV nearly reaches its limit: $\eta_{pV} = \eta_C Z_{pV}$. Figure 9 also shows the role of resonance in achieving high efficiency. When no kinetic energy is produced during a generation event, no optical phonon energy is wasted. Thus, a pV with a resonant bandgap

29

surpasses the TE performance even at lower $\dot{\gamma}^*_{e-p}$.

Finally, Fig. 9 shows the potential of a pV cell to substantially outperform the TE, even at room temperature. Indeed, with a resonant and energetic optical phonon mode which primarily generates electrons, the pV cell triples the efficiency of a TE with $ZT_{\mathrm{TE}} = 1$. Even under reduced nonequilibrium, such a pV cell doubles the TE efficiency. These encouraging results motivate the search for a high Z_{pV} material, which we conduct in Part II[20].

VII. CONCLUSIONS

Here, we proposed and discussed the phonovoltaic cell which harvests energetic optical phonons resonant with the bandgap to generate power in a p-n junction. The central mechanisms, the electron-phonon and anharmonic three-phonon coupling, are discussed to quantify the quantum efficiency ($\eta_{\mathrm{QE}} = \dot{\gamma}^*_{e-p}$). The Monte-Carlo simulations of the Boltzmann transport equation depicts the cell function using these couplings. Then, an approximate efficiency is developed analytically and a pV figure of merit proposed, i.e.,

$$Z_{\mathrm{pV}} = \dot{\gamma}^*_{e-p}\frac{\Delta E_{e,g}}{E_{p,\mathrm{O}}} \leq 1 \quad \dot{\gamma}^*_{e-p} = \frac{\dot{\gamma}_{e-p}}{\dot{\gamma}_{e-p} + \dot{\gamma}_{p-p}},$$

$$\eta_{\mathrm{pV}} \simeq \eta_{\mathrm{C}}Z_{\mathrm{pV}}[1 - 0.75\exp(-\frac{\eta_{\mathrm{C}}\Delta E_{e,g}}{k_{\mathrm{B}}T_c}),$$

$$\eta_{\mathrm{C}} = 1 - \frac{T_c}{T_{p,\mathrm{O}}}. \tag{40}$$

These results are most accurate when the surface recombination is suppressed, hot phonon relaxation is slow compared to the transport (or $L_a = L$), and $\dot{\gamma}^*_{e-p}$ is small or F_F is large. Regardless, Eq. (40) provides reasonable predictive power across a wide range of Z_{pV} and $\eta_{\mathrm{C}}\Delta E^*_{e,g}$, as shown in Figs. 6 and 9. Importantly, this equation shows that either large η_{C} or large Z_{pV} are required for efficient pV operation.

Hydrodynamic simulations highlight the device requirements and validate the analytic model. These requirements are (i) the active volume should be maximized, such that $L_a/L \simeq 1$, unless the relaxation of hot optical phonon populations is slow compared to its transport; (ii) minority carriers must be blocked from entering the contact and recombining (i.e., hindered surface-recombination); (iii) the p-n junction must be sufficiently strong ($\Delta E_{\mathrm{F},p-n} > \eta_{\mathrm{C}}\Delta E_{e,g}$), without inhibiting generation and lowering $\dot{\gamma}^*_{e-p}$. Additionally, the hydrodynamic model predicts that large $\dot{\gamma}^*_{e-p}$ increases the efficiency significantly compared to the linear relationship predicted by the analytic model.

When these requirements are met, and for $Z_{\mathrm{pV}} \geq 0.7$, the pV cell is shown to significantly outperform a TE cell with $Z_{\mathrm{TE}}T = 1$ (Figs. 5, 6, and 9). In Part II[20] of this study, the bandgap of graphite is tuned through partial hydrogenation to resonate with its optical phonon modes in an effort to develop a pV material. However, hydrogenation degrades the electron-phonon coupling and reduces the $\dot{\gamma}^{*}_{e-p}$ below that required for an efficient pV. So, while finding and tuning a high Z_{pV} material remains challenging, Part I of this study shows the benefits of success, and Part II develops the methods for tuning and evaluating a material candidate.

ACKNOWLEDGMENTS

Appendix A: Hydrodynamic Model Simulations

The hydrodynamic model takes the first three moments of the BTE to simulate the electron transport[32]. These moments conserve the carrier density (n_i), momentum density ($\boldsymbol{j}_i$), and kinetic energy density ($\boldsymbol{w}_i$) for electron ($i = e$) and hole ($i = h$), i.e.,

$$\nabla \cdot \boldsymbol{j}_i = e_c \dot{n}_i,$$
$$\boldsymbol{j}_i = \mu_i(\pm k_{\mathrm{B}} T_i \nabla n_i + k_{\mathrm{B}} n_i \nabla T_i - e_c n_i \nabla \varphi_e),$$
$$\nabla \cdot \boldsymbol{w}_i = -\boldsymbol{j_i} \cdot \nabla \varphi - \sum \dot{w}_i, \tag{A1}$$

where T_i and μ_i are the temperature and mobility of carrier i. These equations track the drift and diffusion of electron and hole populations as well as the diffusion and advection of kinetic energy, and $\dot{n}_i$ and $\dot{w}_i$ quantify the addition of carriers and kinetic energy to population i. The kinetic energy flux is

$$\boldsymbol{w}_i = \nabla \frac{3}{2} k_{\mathrm{B}} T_i \boldsymbol{j}_i - \kappa_i \nabla T_i, \tag{A2}$$

where the thermal conductivity is

$$\kappa_i = \frac{\pi^2}{3} \frac{k_B^2}{e_c} T_i \mu_i n_i, \tag{A3}$$

from the Weidemann Franz law.

Here, the electron-phonon interaction drives both $\dot{n}_i$ and $\dot{w}_i$. The generation model follows the band-to-band models[37] discussed previously, i.e.,

$$\dot{n}_i = -a_{e-p}[n_e n_h - n_i(T_{p,O})^2], \tag{A4}$$

where a_{e-p} is the generation coefficient associated with the electron-phonon coefficient and $n_i(T_{p,O})$ is the intrinsic carrier concentration at $T_{p,O}$. The kinetic energy imparted to the electron (and hole) population per generation event is, on average, $(E_{p,O} - \Delta E_{e,g})/2$. The corresponding energy transfer $\dot{s}_G$ is

$$\dot{w}_G = \frac{E_{p,O} - \Delta E_{e,g}}{2} \dot{n}_e. \tag{A5}$$

Additionally, the electron kinetic energy density $(3/2k_B T_e n_e)$ equilibrates with the optical phonon temperature. The corresponding energy transfer is

$$\dot{w}_{i-p,O} = \frac{3}{2} k_B \frac{T_i - T_{p,O}}{\tau_{i-p,E}} n_i, \tag{A6}$$

where $\tau_{i-p,E}$ is the electron phonon energy relaxation time[32].

Furthermore, the Poisson equation ensures a self-consistent simulation, i.e.,

$$\nabla \cdot \epsilon_e \epsilon_\circ \nabla \varphi = -e_c(n_e + n_D - n_h - n_A), \tag{A7}$$

where $\epsilon_e \epsilon_\circ$ is the electrical permittivity of the material and n_D and n_A are the doping densities for electron donor and acceptor atoms.

The optical $(i = p, O)$ and acoustic phonon $(i = p, A)$ populations are modeled using the conduction equation, i.e.,

$$-\nabla \cdot \nabla \kappa_i T_i = \sum \dot{s}_{i-j}, \tag{A8}$$

where the optical phonon population gains energy from an external source $(\dot{s}_{p,O-in})$ and loses energy for each generation event $(\dot{s}_G)$, from heating electron (and hole) $(\dot{s}_{p,O-e})$, and

downconversion ($\dot{s}_{p,\mathrm{O}-p,\mathrm{A}}$), which the acoustic phonon population absorbs, i.e.,

$$\dot{s}_G = E_{p,\mathrm{O}}\dot{n}_e,$$

$$\dot{s}_{p,\mathrm{O}-i} = -\dot{w}_{i-p,\mathrm{O}},$$

$$\dot{s}_{p,\mathrm{O}-p,\mathrm{A}} = E_{p,\mathrm{O}}a_{p-p}[f^\circ_{p,\mathrm{O}}(T_{p,\mathrm{A}})^2 - f^\circ_{p,\mathrm{O}}(T_{p,\mathrm{O}})^2],$$

$$\dot{s}_{p,\mathrm{A}-p,\mathrm{O}} = -\dot{s}_{p,\mathrm{O}-p,\mathrm{A}}, \tag{A9}$$

where $f^\circ_{p,\mathrm{O}}(T)$ is the equilibrium optical phonon occupancy at temperature T, and a_{p-p} is the downconversion coefficient associated with the anharmonic coupling strength. Note that Eq. (A9) assumes that the acoustic phonon populations ($f'^\circ_{p,\mathrm{A}}(T)$ and $f''^\circ_{p,\mathrm{A}}(T)$) are non-degenerate and classical statistics are appropriate, i.e.,

$$f^\circ_{p,\mathrm{O}}(T) = \exp(-\frac{E_{p,\mathrm{O}}}{k_\mathrm{B}T})$$

$$= f'^\circ_{p,\mathrm{A}}(T)f''^\circ_{p,\mathrm{A}}(T). \tag{A10}$$

The hydrodynamic, Poisson, and phonon equations form a set of seven closed balance equations. Note that the closure involves the following assumptions: the kinetic energy is primarily thermal ($w = 3/2k_\mathrm{B}T$), populations are non-degenerate, there is equilibrium within but not between populations e, h, p,O, and p,A, and the temperature tensor is diagonal. If the material is anisotropic care must be taken with the transport coefficients and the assumption of a diagonal temperature tensor; however, the transport has negligible effect on a sufficiently thin pV cell.

1. Boundary Conditions

The optical phonon is excited to a constant temperature in the active region, and it is not allowed to escape at the contacts ($\nabla T_{p,\mathrm{O}} = 0$). (This assumes that the contact material has no optical phonon mode of comparable energy.) All other temperatures are maintained at the contact temperature T_c. An Ohmic contact is simulated for the both carriers when surface recombination occurs (w/SR). Otherwise, the no minority current is allowed to enter the contact and only the majority carrier has its density maintained by the Ohmic contact

(w/o SR), i.e.,

All Simulations:

$$e_c\varphi(0) = E_{\mathrm{F}}(0), \qquad\qquad e_c\varphi(L) = E_{\mathrm{F}}(L) - \Delta\varphi_a,$$

$$\nabla T_{p,\mathrm{O}}(0,L) = 0, \qquad\qquad T_{p,\mathrm{A}}(0,L) = T_e(0,L) = T_h(0,L) = T_c,$$

$$n_h(0) = n_{e,v}\exp\big[\frac{E_{e,v} - E_{\mathrm{F}}(0)}{k_{\mathrm{B}}T_c}\big], \qquad n_e(L) = n_{e,c}\exp\big[\frac{E_{\mathrm{F}}(L) - E_{e,c}}{k_{\mathrm{B}}T_c}\big].$$

w/SR:

$$n_e(0) = n_{e,c}\exp\big[\frac{E_{\mathrm{F}}(0) - E_{e,c}}{k_{\mathrm{B}}T_c}\big], \qquad n_h(L) = n_{e,v}\exp\big[\frac{E_{e,v} - E_{\mathrm{F}}(L)}{k_{\mathrm{B}}T_c}\big].$$

w/o SR:

$$j_e(0) = 0, \ \text{i.e.,} \qquad\qquad j_h(L) = 0, \ \text{i.e.,}$$

$$\nabla T_e(0) = 0, \qquad\qquad \nabla T_h(L) = 0,$$

$$n_e(0) = \frac{k_{\mathrm{B}}T_e}{e_c}\frac{\nabla n_e}{\nabla\varphi_e}, \qquad\qquad \nabla n_h(L) = -\frac{k_{\mathrm{B}}T_h}{e_c}\frac{\nabla n_h}{\nabla\varphi_e}, \qquad\qquad \text{(A11)}$$

where E_{F} is the Fermi energy and $n_{e,c}$ and $n_{e,v}$ are the effective density of states for conduction and valence bands.

2. Simulations

The simulations are performed on a 1-D mesh with 0.25 nm spacing between control volumes. The equations are coupled and solved using the damped-inexact Newton method. Calculations are considered converged when the change in current changes by less than $10^{-6}\%$ over 1000 iterations. Convergence is reached within minutes across a wide range parameters.

Appendix B: Surface Recombination Effects

The negative effects outlined in Section VI B are shown in Fig. B.1. When the generation occurs near the contact, a significant number of minority carriers accumulate in the p-region, as shown in Fig. B.1(a). When these minority carriers are prevented from entering the contact and recombining, they diffuse towards the junction, which separates them from the majority carrier, and then the opposing contact collects them. Conversely, when SR occurs,
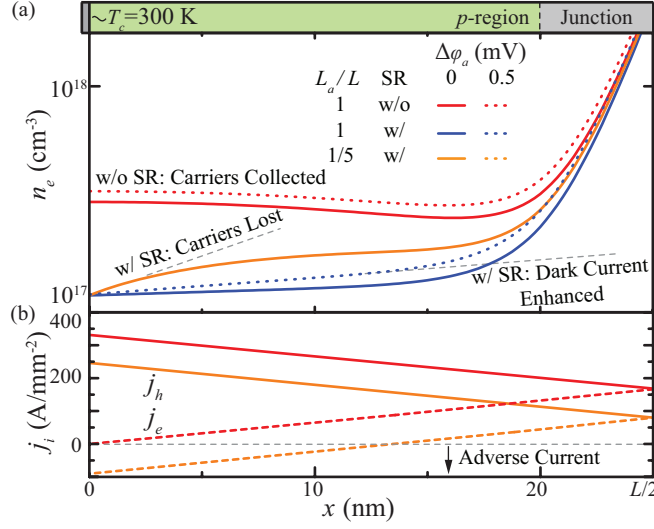
FIG. B.1. (a) Minority carrier density and (b) electron and hole currents in a pV cell with and without surface recombination (SR) for variations in the active volume and applied potential. With SR, carriers generated near the contact are lost instead of being collected. Moreover, the applied voltage drives minority carriers into the contacts, instead of reducing the net generation, reducing pV performance.

these minority carriers diffuse into the adjacent contact as shown in Fig. B.1(a). Indeed, for $L_a = L$, wherein a the large minority density gradient develops at the contact ($x = 0$). This creates a large adverse current near the contact.

While restricting the active region to the junction minimizes this effect, an applied potential drives a substantial number of minority carriers into the contact regardless of L_a/L,as shown in Fig. B.1(a). Thus, an efficient pV cell must utilize window layers on both contacts in order to prevent surface recombination.

* kaviany@umich.edu

[1] H. Goldsmid, *Electronic Refrigeration*, Pion, 1986.

[2] K. Fushinobu, A. Majumdar, and K. Hijikata, ASME J. Heat Transfer **117**, 25 (1995).

[3] M. Bartowiak and G. Mahan, Semiconductors and Semimetals **70**, 245 (2001).

[4] L. da Silva and M. Kaviany, Int. J. Heat Mass Transfer **47**, 2417 (2004).

⁵ M. Hodes, IEEE trans. comp. pack. tech. **33**, 307 (2010).

⁶ G. Span, M. Wagner, T. Grasser, and L. Holmgren, Phys. Stat. Sol. (RRL) **1**, 241 (2007).

⁷ M. Wagner, G. Span, S. Holzer, and T. Grasser, Semiconductor Sci. and Tech. **22**, S173 (2007).

⁸ R. Chavez et al., Mat. Res. Soc. Symp. Proc. **1543**, 3 (2013).

⁹ A. Becker, R. Chavez, N. Petermann, G. Schierning, and R. Schmechel, Mat. Res. Soc. Symp. Proc. **691**, G8.37.1 (2002).

¹⁰ R. Chavez et al., J. Elec. Mat. **43**, 2376 (2014).

¹¹ X. Ruan and M. Kaviany, Phys. Rev. B **73**, 155422 (2006).

¹² X. Ruan and M. Kaviany, J. Heat Transfer **129**, 3 (2007).

¹³ S. Shin, C. Melnick, and M. Kaviany, Phys. Rev. B **87**, 075317 (2013).

¹⁴ S. Shin and M. Kaviany, Phys. Rev. B **91**, 85301 (2015).

¹⁵ O. Madelung, *Semiconductors: Data Handbook*, Springer, 2004.

¹⁶ S. R. J. Maultzsch, C. Thomsen, H. Requardt, and P. Odejón, Phys. Rev. Lett. **92**, 075501 (2004).

¹⁷ S. Piscanec, M. Lazzeri, F. Mauri, A. Ferrari, and J. Robertson, Phys. Rev. Lett. **93**, 185503 (2004).

¹⁸ N. Bonini, Lazzeri, N. Marzari, and F. Mauri, Phys. Rev. Lett. **99**, 176802 (2007).

¹⁹ V. Georgakilas et al., Chem. Rev. **112**, 6156 (2012).

²⁰ C. Melnick and M. Kaviany, Phys. Rev. B , This issue (2015).

²¹ J. Sofo, A. Chaudhari, and G. Barker, Phys. Rev. B **75**, 153401 (2007).

²² H. Peelaers, A. Hernández-Nieves, O. Leenaerts, B. Partoens, and F. Peeters, App. Phys. Lett. **98**, 051914 (2011).

²³ M. Pumera and C. Hong, Chem. Soc. Rev. **42**, 5987 (2013).

²⁴ J. Gordon, Am. J. Phys. **59**, 551 (1991).

²⁵ *Handbook of Photovoltaic Science and Engineering*, Wiley, 1984.

²⁶ M. Kaviany, *Heat Transfer Physics*, Cambridge University Press, 2nd edition, 2014.

²⁷ A. Martií and G. Araújo, Solar En. Mat. and Solar Cells **43**, 203.

²⁸ S. Baroni, S. de Gironcoli, A. D. Corso, and P. Giannozzi, Rev. Mod. Phys. **73**, 515 (2001).

²⁹ G. Srivistava, *The Physics of Phonons*, Adam Hilger, 1990.

³⁰ D. Ecsedy and P. Klemens, Phys. Rev. B **15**, 5957 (1976).

³¹ O. Hellman and I. Abrikosov, Phys. Rev. B **67**, 144304 (2003).

[32] M. Lundstrom, *Fundamentals of Carrier Transport*, Cambridge Univ. Press, 2nd edition, 2000.

[33] W. Shockley and H. Queisser, J. of Appl. Phys. **32**, 510 (1961).

[34] A. J. Nozik, Ann. Rev. of Phys. Chem. **52**, 193 (2001).

[35] For example, a properly doped, large bandgap material (window layer) placed between contact and pV material blocks minority carriers from entering the contact while enabling majority carrier transport.

[36] Note that this is physically impossible: If the electron-phonon coupling is completely inhibited by the dark current, the phonon-phonon or intraband electron-phonon couplings must contribute to the relaxation of the optical phonon mode.

[37] W. Shockley, Bell Sys. Tech. J. **28**, 435 (1949).